The Generation of Packets of Hairpins From Pairs of Counter-Rotating Vortices In Shear Flows

Jacob Cohen[1], Michael Karp[1] and Ilia Shukhman[2]

[1] *Faculty of Aerospace Engineering*
Technion - Israel Institute ofTechnology
Haifa 32000, Israel

[2] *Institute of Solar–Terrestrial Physics*
Russian Academy of Sciences, Siberian Department
Irkutsk 664033, P.O. Box 4026, Russia

In the present work we follow the breakdown of pairs of counter-rotating vortices (CVP) and the consequence formation of packets of hairpins in uniform shear flows. We employ a recent developed method which is capable of following (numerically) the evolution of finite-amplitude localized vortical disturbances embedded in shear flows. The solution is carried out using Lagrangian variables in Fourier space which is convenient and enables fast computations on a regular PC. Streamwise variation of the CVP is required to generate concentrated spanwise vorticity which together with the lift-up by the induced velocity and shear of the base flow generates packets of hairpins. This scenario, obtained 'synthetically' with minimal simple elements seems to be universal and may explain similar observations both in fully developed wall-bounded shear flows as well as in wall-bounded transitional shear flows. This work has been motivated by our previous observation, based on experimental, numerical and theoretical results, that the formation and characteristics associated with the structure of a single hairpin, evolved from a dipole vortex, are very similar to the structures of those composing packets of hairpins in turbulent and transitional shear flows.

1 Introduction

During the last fifty years it has become clear that although wall bounded turbulent shear flows are characterized by unsteady, seemingly chaotic motion, in fact, however, the motion is not random and it has been observed to be governed by well organized coherent vortical structures. In particular, the observation of counter-rotating streamwise vortices (CVP's), which lead to the formation of low and high-speed velocity regions (streaks), observed in the near wall region, and hairpin-shaped vortices extending across the boundary layer. Since their first experimental identification by Kline *et al.* (1), these coherent structures have come under intense investigations regarding their characterization, generation and sustenance mechanisms (e.g (2; 3)). The presence of streaky structures and their further breakup and appearance of packet of hairpin vortices has been also observed in transitional flows (e.g in laminar boundary layers (4); pipe flow (5); subcritical channel flow (6; 7)).

The similarity of the coherent structures naturally occurring in different fully developed boundary turbulent shear flows as well as in transitional flows and free shear layers suggests the existence of a basic mechanism responsible for the formation of these structures, under various base flow conditions. The common elements for all such flows are the *shear of the base flow* and the presence of a *localized vortical disturbance.* Recently, combining experimental, numerical and theoretical efforts, it was demonstrated (8; 9; 10; 11; 12) that a simple model, which takes into account only the interaction between a localized vortical disturbance and a laminar shear base flow, is capable of reproducing the generation process and characteristics of the coherent structures. For the case in which the vortical disturbance is superimposed on pure shear flow, the results (11; 7) have shown that independent of the initial disturbance geometry a small amplitude vortical disturbance eventually evolves into a pair of streamwise vortices, whereas, a sufficiently large amplitude disturbance evolves into a hairpin. Moreover, other characteristics such as the spanwise separation between the two elongated vortical regions (expressed in terms of wall units), the inclination angle of the hairpins and their convective velocity correspond well to those observed in turbulent wall bounded shear flows.

The investigations of the development and characterization of the key coherent structures, both experimentally and numerically have progressed primarily in two different but complementary directions. First, the study of coherent structures in fully turbulent/transitional flows, and second, the investigation of structures in 'quiet' laminar base flows by following artificially generated disturbances. The former has the advantage of being the 'real' flow but the process of investigation is complicated by the noise that is inherent in any turbulent flow and by the complexity of extraction of the embedded coherent structures. The later is more suitable to isolate the major effects associated with the coherent structures and is thus effective to study their formation, growth and decay/breakdown. The major disadvantage is that the base flow lacks the high shear stress that is associated with the turbulent flows and the mutual interaction of the coherent structures.

In this article we pursue the second method of investigation by following the minimal sequence of events required for the generation of packets of hairpins due to the breakup of synthetic pair of CVP superimposed on a uniform base shear flow. For this purpose we employ our recent developed method which is capable of following (numerically) the evolution of finite-amplitude localized vortical disturbances embedded in shear flows (13). An experimental example of the streaks breakdown and consequent formation of hairpins process

Vertical Plane

Horizontal Plane
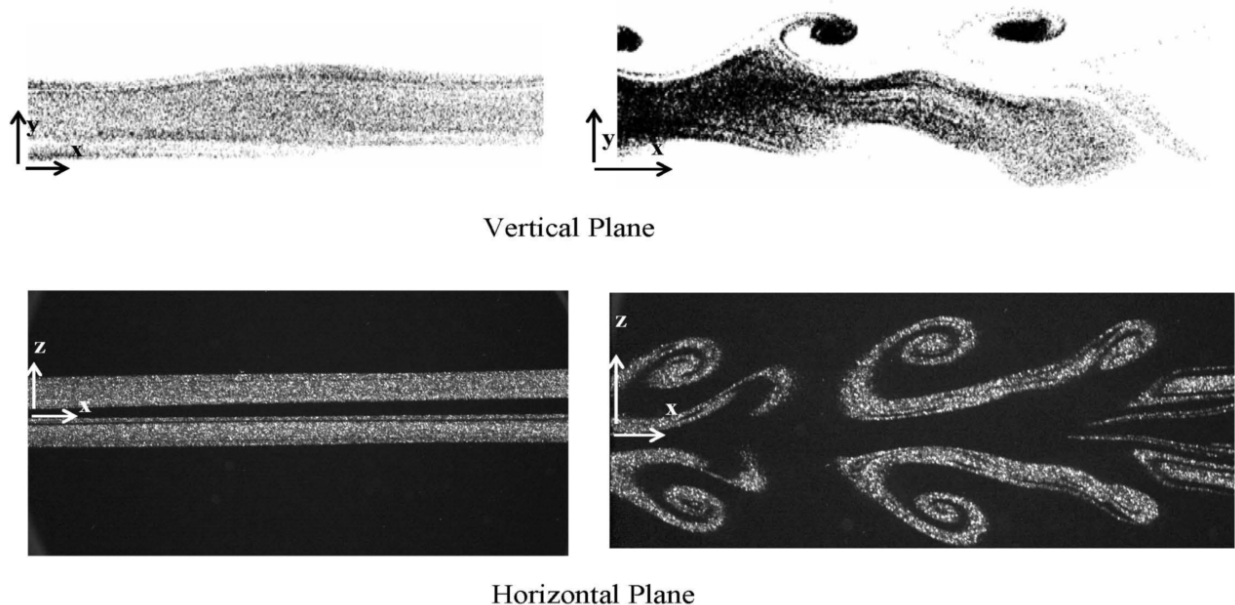
Figure 1: Visualization of streaky structures and their further breakup and formation of packet of hairpins in sub-critical horizontal channel flow. Data taken from (6), $Re = 1667$, $V_{inj} = 0.29$

in subcritical channel flow (6; 7) is shown figure in 1, where for a given Reynolds number (based on the centerline velocity and half-channel height) the breakdown of the streaks depends on the nondimensional injection velocity (normalized by the centerline velocity) through the bottom wall.

2   Mathematical-numerical approach

2.1   Problem formulation

We consider the evolution of a localized vortical disturbance. Accordingly, the initial disturbed vorticity is assumed to be confined to a small region in the flow field. Since the advection of the small disturbed region as a whole is not of interest, we use a Galilean frame, moving with the disturbance, instead of the laboratory frame. Taking advantage of the smallness of the disturbed region, the base flow velocity can be represented to leading order by its gradient tensor. Here we focus on the case of pure shear for which the velocity and vorticity vectors (in a cartesian system, x, y and z), are respectively given by

$$\boldsymbol{V} = (-\Omega y,\, 0,\, 0)\,, \quad \boldsymbol{\Omega} = (0,\, 0,\, \Omega)\,, \tag{1}$$

where Ω is a constant representing the vorticity of the base flow. The equation describing the evolution of vorticity ($\boldsymbol{\omega}$) associated with a 3D finite-amplitude localized disturbance in

incompressible viscous base flow is

$$\frac{\partial \boldsymbol{\omega}}{\partial t} + (\boldsymbol{V} \cdot \boldsymbol{\nabla}) \, \boldsymbol{\omega} - (\boldsymbol{\omega} \cdot \boldsymbol{\nabla}) \boldsymbol{V} - (\boldsymbol{\Omega} \cdot \boldsymbol{\nabla}) \, \boldsymbol{v} = \nu \, \Delta \boldsymbol{\omega} + (\boldsymbol{\omega} \cdot \boldsymbol{\nabla}) \, \boldsymbol{v} - (\boldsymbol{v} \cdot \boldsymbol{\nabla}) \, \boldsymbol{\omega}, \tag{2}$$

where t is time, ν the kinematic viscosity and the disturbance vorticity $\boldsymbol{\omega}$ and velocity $\boldsymbol{v}$ are related by $\boldsymbol{\omega} = \nabla \times \boldsymbol{v}$.

In what follows it is convenient to interchangeably associate the cartesian coordinates x, y and z with the subscripts 1, 2 and 3, respectively. Substituting (1) into (2), the three equations for the three disturbance vorticity components are

$$\mathcal{L}\omega_1 - \Omega \frac{\partial v_3}{\partial x_1} = \nu \Delta \omega_1 + N_1, \tag{3a}$$

$$\mathcal{L}\omega_2 + \Omega \, \omega_1 - \Omega \frac{\partial v_3}{\partial x_2} = \nu \Delta \omega_2 + N_2, \tag{3b}$$

$$\mathcal{L}\omega_3 - \Omega \frac{\partial v_3}{\partial x_3} = \nu \Delta \omega_3 + N_3, \tag{3c}$$

where $\mathcal{L}$ is the convective operator:

$$\mathcal{L} = \frac{\partial}{\partial t} + V_1 \frac{\partial}{\partial x_1} = \frac{\partial}{\partial t} - \Omega \, x_2 \frac{\partial}{\partial x_1}, \tag{4}$$

and N_m, $m = 1, 2, 3$ represent the corresponding nonlinear terms, i.e

$$N_m = \omega_n \frac{\partial v_m}{\partial x_n} - v_n \frac{\partial \omega_m}{\partial x_n}, \tag{5}$$

for which the summation convention is applied.

2.2 Transformation into Fourier space

The set of equations (3) are first Fourier transformed via

$$\hat{f}_m(\boldsymbol{k}) = \frac{1}{(2\pi)^3} \int f_m(\boldsymbol{r}) \, \exp\left(-i\boldsymbol{k}\,\boldsymbol{r}\right) d^3x, \quad f_m(\boldsymbol{r}) = \int \hat{f}_m(\boldsymbol{k}) \, \exp\left(i\boldsymbol{k}\,\boldsymbol{r}\right) d^3k, \tag{6}$$

where m=1,2,3, $\hat{f}_m(\boldsymbol{k})$ being the Fourier transform and $f_m(\boldsymbol{r})$ its inverse transform, $\boldsymbol{r} = (x, y, z)$ is the real space physical vector and $\boldsymbol{k}$ its corresponding wave number vector in Fourier space. The resulted set of equations is:

$$\mathcal{L}_k \hat{\omega}_1(\boldsymbol{k}) - ik_1\Omega\hat{v}_3(\boldsymbol{k}) = -\nu k^2 \hat{\omega}_1(\boldsymbol{k}) + \hat{N}_1(\boldsymbol{k}), \tag{7a}$$

$$\mathcal{L}_k \hat{\omega}_2(\boldsymbol{k}) + \Omega \, \hat{\omega}_1(\boldsymbol{k}) - ik_2\Omega\hat{v}_3(\boldsymbol{k}) = -\nu k^2 \hat{\omega}_2(\boldsymbol{k}) + \hat{N}_2(\boldsymbol{k}), \tag{7b}$$

$$\mathcal{L}_k \hat{\omega}_3(bk) - ik_3\Omega\hat{v}_3(\boldsymbol{k}) = -\nu k^2 \hat{\omega}_3(\boldsymbol{k}) + \hat{N}_3(\boldsymbol{k}), \tag{7c}$$

where $k^2 = k_1^2 + k_2^2 + k_3^2$ and the operator $\mathcal{L}_k$ is given by

$$\mathcal{L}_k = \frac{\partial}{\partial t} + \Omega k_1 \frac{\partial}{\partial k_2}. \tag{8}$$

The Fourier transform of each one of the products included in N_m (see 5) is the convolution of the corresponding Fourier transforms. Thus the expression for $\hat{N}_m(\boldsymbol{k})$ can be written as:

$$\hat{N}_m(\boldsymbol{k}) = i \int d^3k' \left\{ k_n \left[v_m(\boldsymbol{k}') \, \omega_n(\boldsymbol{k} - \boldsymbol{k}') - v_n(\boldsymbol{k}') \, \omega_m(\boldsymbol{k} - \boldsymbol{k}') \right] \right\}. \tag{9}$$

2.3   Transition into Lagrangian variables in $\boldsymbol{k}$-space

Following (9) the resulted set of equations (7) is expressed in terms of Lagrangian co-ordinates in the Fourier space. For this, we demand that the operator $\mathcal{L}_k$ be the substantial derivative along an unperturbed trajectory in $\boldsymbol{k}$- space, i.e,

$$\mathcal{L}_k = \frac{\partial}{\partial t} + \Omega\, k_1\, \frac{\partial}{\partial k_2}$$

$$\equiv \frac{d}{dt} = \frac{\partial}{\partial t} + \frac{dk_1}{dt}\frac{\partial}{\partial k_1} + \frac{dk_2}{dt}\frac{\partial}{\partial k_2} + \frac{dk_3}{dt}\frac{\partial}{\partial k_3}. \tag{10}$$

This leads to the following set of equations describing the temporal evolution of the wave vector $\boldsymbol{k}$:

$$\frac{dk_1}{dt} = 0, \quad \frac{dk_2}{dt} = \Omega\, k_1, \quad \frac{dk_3}{dt} = 0, \tag{11}$$

the solution of which is:

$$k_1 = q_1, \quad k_2 = \Omega\, t\, q_1 + q_2, \quad k_3 = q_3, \tag{12}$$

where the initial value of $\boldsymbol{k}(t=0) = \boldsymbol{q}$.

Designating,

$$\zeta(\boldsymbol{q}, t) = \hat{\omega}\Big(\boldsymbol{k}(\boldsymbol{q}, t), t\Big), \tag{13}$$

and utilizing the simple algebraic relation between the Fourier transformed velocity and vorticity vectors, i.e,

$$\hat{\boldsymbol{v}}(\boldsymbol{k}) = i\, k^{-2}\Big[\boldsymbol{k} \times \hat{\boldsymbol{\omega}}(\boldsymbol{k})\Big], \tag{14}$$

lead to the following final set of equations:

$$\frac{d\zeta_1(\boldsymbol{q}, t)}{dt} = -\Omega\, k^{-2}\, k_1 \Big[k_1\, \zeta_2(\boldsymbol{q}, t) - k_2\, \zeta_1(\boldsymbol{q}, t)\Big] - \nu\, k^2\, \zeta_1(\boldsymbol{q}, t) + \hat{N}_1(\boldsymbol{q}, t), \tag{15a}$$

$$\frac{d\zeta_2(\boldsymbol{q}, t)}{dt} = -\Omega\, \zeta_1(\boldsymbol{q}, t) - \Omega\, k^{-2}\, k_2 \Big[k_1\, \zeta_2(\boldsymbol{q}, t) - k_2\, \zeta_1(\boldsymbol{q}, t)\Big] - \nu\, k^2\, \zeta_2(\boldsymbol{q}, t) + \hat{N}_2(\boldsymbol{q}, t), \tag{15b}$$

$$\frac{d\zeta_3(\boldsymbol{q}, t)}{dt} = \Omega\, k^{-2}\, k_3 \Big[k_1\, \zeta_2(\boldsymbol{q}, t) - k_2\, \zeta_1(\boldsymbol{q}, t)\Big] - \nu\, k^2\, \zeta_3(\boldsymbol{q}, t) + \hat{N}_3(\boldsymbol{q}, t). \tag{15c}$$

2.4   Numerical procedure

The advantage of the theoretical model described above is that the nonlinear partial differential equations for the vorticity disturbance in the physical space are replaced by corresponding ordinary nonlinear equations. In the following a simple numerical procedure is outlined for solving these equations. We first choose the initial vortical disturbance in the physical space, transform it into Fourier space where we perform numerical integration of the Lagrangian variables, and finally, at a predetermined time, the spatial structure of the disturbance vorticity in the physical space is obtained by executing an inverse Fourier transform back to the physical space. For a given initial vortex the final solution is obtained (within minutes on a standard laptop) using the software, Matlab. It is noted that, for a similar calculation, the time required with the commercial software Fluent is more than two orders of magnitude.

2.4.1 Initial conditions and flow parameters

We consider three different initial conditions associated respectively with the development of a single hairpin from a localized Gaussian vortex, two hairpins from the streamwise edges of an elongated Gaussian vortex and the formation of a packet of hairpins from a pair of counter-rotating streamwise vortices subjected to streamwise waviness of a spanwise vortex sheet. The first two cases have already been demonstrated by (11) using the Fluent software and are included here for the sake of completeness and comparison

The vorticity field of a localized Gaussian vortex and its Fourier transform are respectively given by

$$\boldsymbol{\omega}(\boldsymbol{r}, t = 0) = \nabla F \times \boldsymbol{P}_0, \quad F = (\pi^{1/2}\delta)^{-3} \exp(-r_s^2/\delta^2), \tag{16}$$

$$\hat{\boldsymbol{\omega}}(\boldsymbol{k}, t = 0) = \zeta(\boldsymbol{q}, t = 0) = \frac{i}{(2\pi)^3}(\boldsymbol{q} \times \boldsymbol{P}_0) \exp\left(-\tfrac{1}{4}q^2\delta^2\right), \tag{17}$$

where r_s is the spherical radial co-ordinate, δ is the representative length scale of the disturbance and $\boldsymbol{P}_0$ is its initial fluid impulse. The strength of the initial vortex is characterized by $\varepsilon = \omega_{\max}(t = 0)/|\Omega|$, where $\omega_{\max}(t = 0) = 0.154|\boldsymbol{P}_0|/\delta^4$ for the Gaussian vortex and $\omega_{\max}(t) = \max|\boldsymbol{\omega}(\boldsymbol{r}, t)|$. The magnitude of ε is used to describe an initial vortex as linear ($\varepsilon << 1$) or nonlinear. The effect of viscosity is represented by the 'vortex Reynolds number', $\mathrm{Re} = |\Omega|\delta^2/\nu$. For all cases described below we set the parameters to be $\Omega = 40[1/s]$, $\delta = 0.001[m]$ and $\mathrm{Re} = 40$. Nonlinearity is essential for the formation of hairpins and hence we choose $\varepsilon = 7.5$ for the first two cases and $\varepsilon = 3.75$ for the third one.

The second shape of the initial disturbance is that of a horizontal streamwise elongated Gaussian vortex. Its vorticity field is also defined by equation (16), except for the spherical radial coordinate r_s which is replaced by r_e, the expression for which is given by:

$$r_e = \sqrt{\bar{x}^2 + y^2 + z^2}, \quad \bar{x} = \begin{cases} x - L; & |x| > L, \ x > 0 \\ x + L; & |x| > L, \ x < 0 \\ 0; & |x| < L, \end{cases} \tag{18}$$

where the ratio L/δ determines the disturbance initial elongation. When this ratio equals to zero, the initial disturbance reduces to that of the Gaussian vortex (equation 16), whereas for a sufficiently large ratio, it can be approximately considered as a 'streamwise independent' disturbance. Here we present results for $L/\delta = 5$ and $L/\delta = 10$.

The third case is a superposition of an initial CVP and a wavy spanwise vortex sheet. The expression for the initial CVP is:

$$\omega_x = \varepsilon\,\Omega\,\exp\left(-y^2/\delta^2\right) \cdot \left\{\exp\left(-(z - d_0)^2/\delta^2\right) + \exp\left(-(z + d_0)^2/\delta^2\right)\right\}, \tag{19}$$

where the separation distance between the centers of the two streamwise vortices is $2d_0 = 2\delta$. The expression for the spanwise vortex sheet is:

$$\omega_z = a_0\,\Omega \cdot \exp\left\{-\left[y - h_0 \cdot \cos(2\pi\,x/\lambda)\right]^2/\delta^2\right\}, \tag{20}$$

where the constants are set to be $a_0 = 0.5$, $h_0/\delta = 0.5$ and $\lambda/\delta = 10$. Scematic 3D views of the intial vortical structures are shown in figure 2.
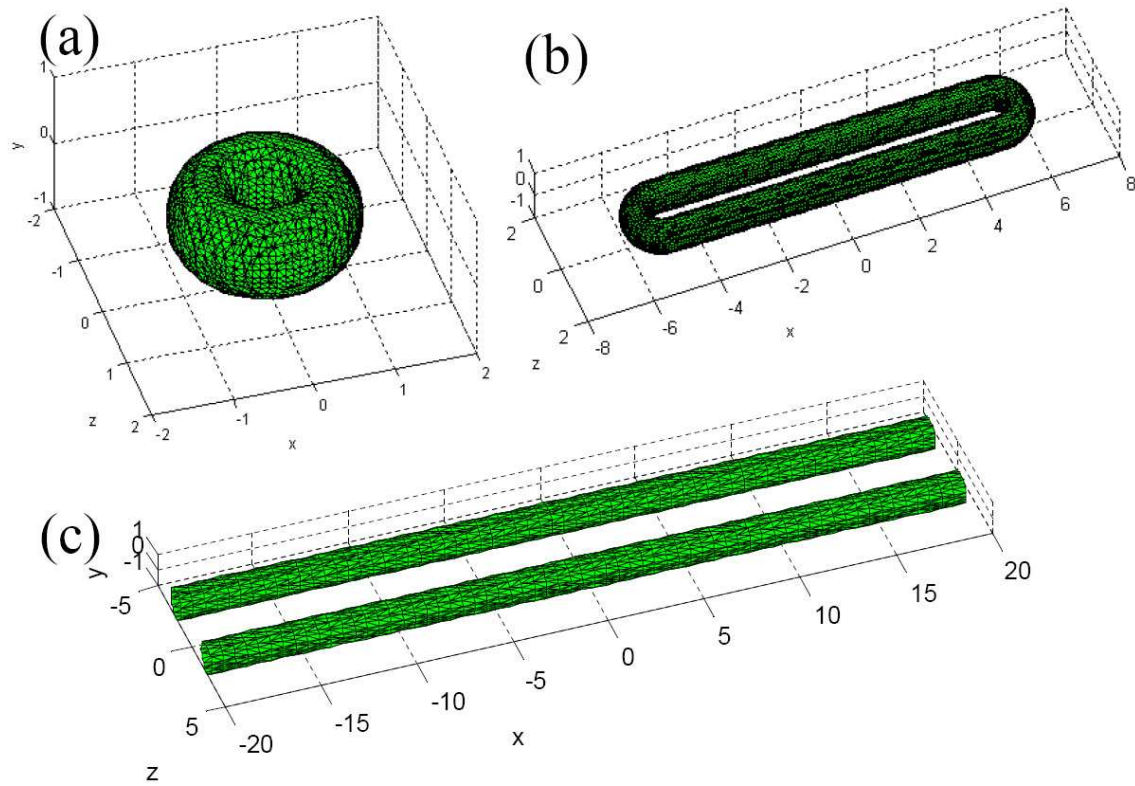
Figure 2: Schematic 3D views of the initial vortices; (a) Gaussian vortex; (b) streamwise elongated vortex; (c) CVP.

2.4.2 Numerical integration and calculation of the vorticity components in the physical space

After the initial vorticity field is transformed into the Fourier space, Eq. (15) is integrated in time using the Euler method. The evaluation of the convolution sums in the nonlinear terms on the right hand sides of (15) is carried out by utilizing a pseudospectral transform method (e.g. (14; 15)).

The vorticity components ω_m in the physical space is given by

$$\omega_m(\boldsymbol{r}, t) = \int d^3k \, \hat{\omega}_m(\boldsymbol{k}, t) \, e^{i\mathbf{k}\mathbf{r}}. \tag{21}$$

However, this is not a straight forward step because the wave-number vector $\boldsymbol{k}$ depends on time. To avoid this difficulty the relation between the physical coordinates $\boldsymbol{r}_0 = (x_0, y_0, z_0)$, indicating the coordinates of the initial position of a fluid particle at time $t = 0$ and the coordinates $\boldsymbol{r} = (x, y, z)$ where the same particle has arrived at time t (following an unperturbed trajectory), has to be derived. To do so we first pass from integration in $\boldsymbol{k}$ space to integration in $\boldsymbol{q}$, using the incompressibility condition, i.e, $d^3k = d^3q$, and the relation

$$\boldsymbol{k} \cdot \boldsymbol{r} = \boldsymbol{q} \cdot \boldsymbol{r}_0. \tag{22}$$

Finally we obtain

$$\omega_m(\boldsymbol{r}, t) = \omega_m\big(\boldsymbol{r}_0(\boldsymbol{r}, t)\big) = \int d^3q \, \zeta_m(\boldsymbol{q}, t) \, e^{i\,[q_1\,x_0(\mathbf{r},\,t) + q_2\,y_0(\mathbf{r},\,t) + q_3\,z_0]}, \tag{23}$$

where the relation between the initial position of the fluid particle and the position at time t, is given by:

$$x_0 = x + \Omega\,t\,y, \quad y_0 = y, \quad z_0 = z. \tag{24}$$

3 Results

In the following the evolution of the three initial vortical fields is described. The resulted vortex structures are identified by plotting various threshold levels of the vorticity magnitude or by plotting iso-surfaces of the second invariant Q of the velocity gradient tensor [1] (e.g. (16), (17)). Length and time scales are normalized by δ and $1/|\Omega|$, respectively, and denoted by capital letters.

When a strong initial Gaussian vortex ($\varepsilon = 7.5$) is initially placed in simple shear the evolved structure is that of a hairpin vortex. The hairpin obtained at $T = 5$ by the current method (figure 3b) is compared with the one obtained by (11) using CFD software (figure 3a). The two structures look the same.

In figure 4 the evolved structure of an initially elongated vortex is presented for $L/\delta = 5$ at $T = 4.5$ (figure 4a) and for $L/\delta = 10$ at $T = 5$ (figure 4b). Above a certain ratio of L/δ, two hairpins (at most) are formed at both streamwise ends of the elongated vortex. (The reader is referred to the discussion in (11) regarding the vortex dynamics in this case).
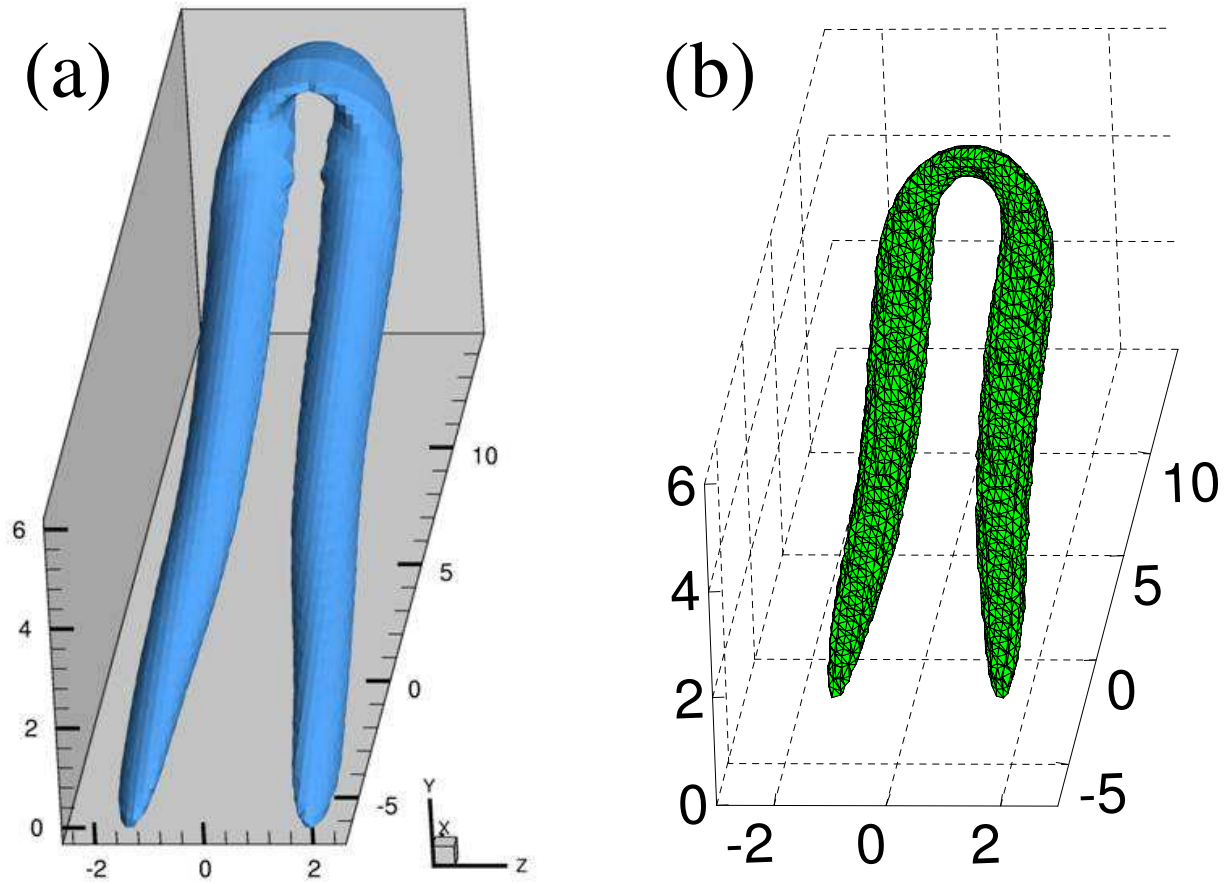
Figure 3: Single hairpin evolved from an initial Gaussian vortex. The structure at $T = 5$ is shown by iso-surface according to the Q definition for $Q/Q_{max} = 0.5$. (a) obtained by (11) using CFD software; (b) obtained by the current method.
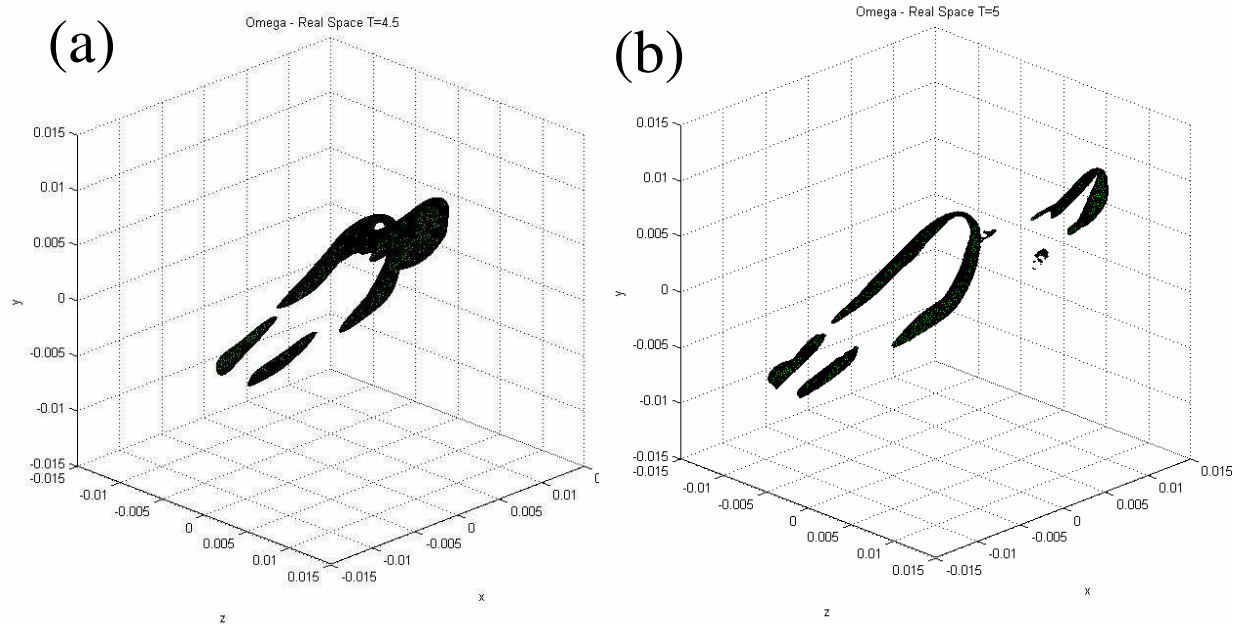
Figure 4: Pair of hairpins evolved from an initially elongated vortex. The structures are shown by vorticity iso-surface of $\omega/\omega_{max} = 0.5$. (a) $L/\delta = 5$, $T = 4.5$; (b) $L/\delta = 10$, $T = 5$.

Thus, even an infinitely long pair of counter-rotating vortex pair (CVP), similar to the one presented in figure 2c, can only produce two hairpins.

Therefore, in order to generate a packet of hairpins an additional flow element is required to introduce streamwise variation of the CVP. This is done by adding a wavy (in x) spanwise vortex sheet. The (vertically) induced velocity by the CVP distorts the based flow and results in an inflectional instability which further enhances the streamwise undulation of the vortical structures and leads to the formation of a packet of hairpins (figure 5). By $T = 1.5$ (figure 5a) the streamwise waviness of the CVP is already observed, corresponding to the imposed streamwise wavelength of the spanwise vortex sheet. By $T = 2$ (figure 5b) the waviness is distorted and the CVP seems to be composed of six periodical elements. Consequently, at $T = 2.5$ (figure 5c) a spanwise vortex segment is formed above the regions connecting two consecutive streamwise elements of the CVP. With time the top spanwise vortical segments are widen and join the streamwise vortical elements situated beneath them. Consequently, a packet of hairpins is formed (see $T = 3.5$ and $T = 4$ in figures 5a and 5b, respectively). This scenario seems to be universal and may explain similar observations in fully developed wall-bounded shear flows as well as in wall-bounded transitional shear flows (e.g. (18).)

In order to follow the inclination angle of the evolved packet, side views of the 'bridges' connecting the top spanwise vortical segments ('heads') with the bottom streamwise vortical 'legs', are shown in figure 6. It can be seen that by $T = 5$ the inclination angle is about 45°, which agrees with previous observations of hairpins in turbulent boundary layers.

---

[1] $Q = -\frac{1}{2}A_{mn}A_{nm}$, where $A_{ij} = \partial v_i/\partial x_j$.

9
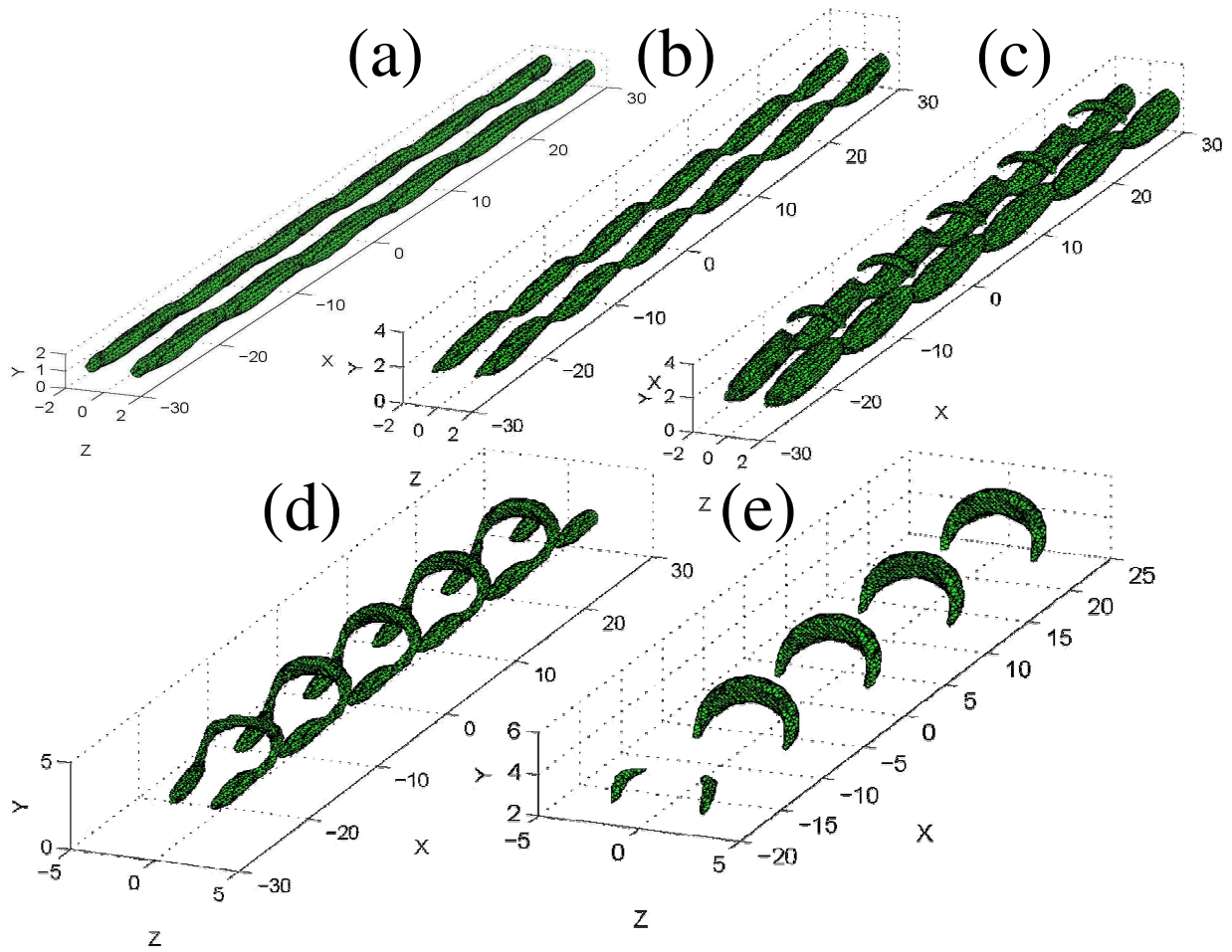
Figure 5: The temporal evolution of a packet of hairpins from a wavy spanwise vortex sheet imposed on a CVP. The structures are shown by iso-surfaces according to the Q definition. (a) $T = 1.5$, $Q/Q_{max} = 0.6$; (b) $T = 2$, $Q/Q_{max} = 0.6$; (c) $T = 2.5$, $Q/Q_{max} = 0.3$; (d) $T = 3.5$, $Q/Q_{max} = 0.3$; (e) $T = 4$, $Q/Q_{max} = 0.3$.
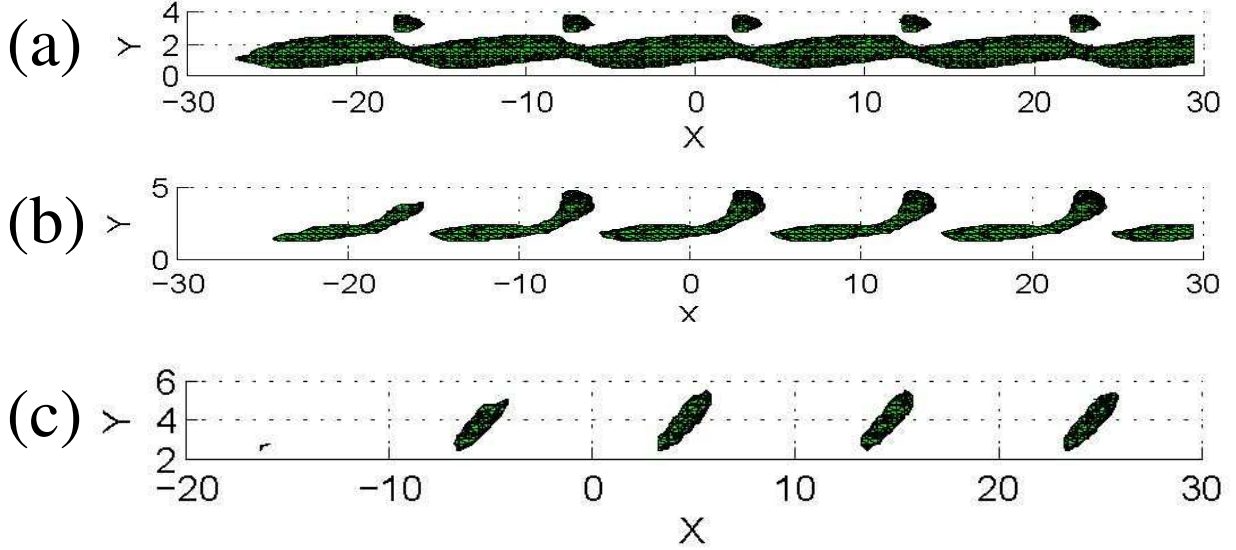
Figure 6: Side views of the temporal evolution of a packet of hairpins from a wavy spanwise vortex sheet imposed on a CVP. The structures are shown by iso-surfaces according to the Q definition, $Q/Q_{max} = 0.1$. (a) $T = 2.5$; (b)T=3.5; (c) $T = 5$.

4 Conclusions

The evolution of localized vortical disturbances in homogenous shear can lead to the development of key structures (e.g. CVPs and hairpin vortices) that have been observed in turbulent and transitional shear flows. We have developed an efficient analytical-based method which allows to predict the nonlinear evolution of localized vortices in planar homogenous shear flow. In this novel method, the solution is carried out using Lagrangian variables in Fourier space. Using this method, it is shown that an initially Gaussian vortex evolves into a single hairpin, whereas an initially elongated vortex evolves into a pair of hairpins formed in its upstream and downstream edges. To generate a packet of hairpins, a streamwise-wavy spanwise vortex sheet must be added to an initial CVP. The streamwise wavelenghth of the spanwise sheet determines the number of hairpins in the packet. The undulation of the CVP is naturally strengthened due to the inflectional instability of the base flow caused by its distortion when the induced velocity of the CVP becomes significant. The formation of the hairpins begins by the generation of spanwise vortex segments above the region connecting two consecutive elements of the resulting streamwise-periodic CVP. Side views of the hairpins show that their inclination angle relative to the base flow is 45° which agrees with previous observations of hairpins in turbulent boundary layers.

11

References

[1] S. J. Kline, W. C. Reynolds, F. A. Schraub, P. W. Runstadler, The structure of turbulent boundary layers, J. Fluid Mech. 30 (1967) 741–773.

[2] S. K. Robinson, Coherent motions in the turbulent boundary layers, Ann. Rev. Fluid Mechanics 23 (1991) 601–639.

[3] R. L. Panton, Self-Sustaining Mechanisms of Wall Turbulence, Computational Mechanics Publications, Southampton, 1997.

[4] M. S. Acarlar, C. R. Smith, A study of hairpin vortices in a laminar boundary layer.Part 1. Hairpin vortices generated by a hemisphere protuberance, J. Fluid Mech. 175 (1987) 1–41.

[5] J. Cohen, J. Philip, G. Ben-Dov, Aspects of linear and nonlinear instabilities leading to transition in pipe and channel flows, Phil. Trans. R. Soc. A 367 (2009) 509527.

[6] A. Svizher, Experimental study of the evolution of the coherent structures in wall bounded shear flows using hpiv, PhD Thesis Technion-Israel Institute of Technology.

[7] A. Svizher, J. Cohen, Holographic particle image velocimetry measurements of hairpin vortices in a subcritical air channel flow, Phys. Fluids 18 (2006) 014105.

[8] J. Cohen, V. Suponitsky, P. Z. Bar-Yoseph, A. Svizher, J. Philip, Localized disturbances and their relation to turbulent shear flows, AIAA-3226, Proceedings of the 36th AIAA Fluid Dynamics Conference and Exhibit, San Francisco, California, USA.

[9] I. G. Shukhman, Evolution of a localized vortex in plane nonparallel viscous flows with constant velocity shear: I. Hyperbolic flow, Phys. Fluids 18 (2006) 097101.

[10] I. G. Shukhman, Evolution of a localized vortex in plane nonparallel viscous flows with constant velocity shear: II. Elliptic flow, Phys. Fluids 19 (2007) 017106.

[11] V. Suponitsky, J. Cohen, P. Z. Bar-Yoseph, The generation of streaks and hairpin vortices from a localized vortex embedded in unbounded uniform shear flow, J Fluid Mech 535 (2005) 65–100.

[12] J. Philip, J. Cohen, The evolution of a finite-amplitude localized disturbance in an irrotational unbounded plane stagnation flow, J. Fluid Mech. 555 (2006) 459 – 473.

[13] J. Cohen, I. G. Shukhman, M. Karp, J. Philip, The evolution of finite-amplitude localized vortices in homogenous shear, AIAA-2008-4419 invited paper, Proceedings of the 5th AIAA Theoretical Fluid Mechanics Conference, Seattle, Washington, USA.

[14] S. A. Orszag, Numerical simulation of incompressible flows within simple boundaries: I, galerkin (spectral) representations, Stud. Appl. Math. 50 (1970) 293–327.

[15] S. A. Orszag, Transform method for calculation of vector coupled sums: Application to the spectral form of the vorticity equation, J. Atmosph. Sci. 28 (1970) 1074.

[16] J. C. R. Hunt, A. A. Wray, P. Moin, Eddies, stream, and convergence zones in turbulent flows, Center for Turbulence Research, Stanford Univ., Report CTR-S88 (1988) 193.

[17] B. J. Cantwell, On the behavior of velocity gradient tensor invariants in direct numerical simulations of turbulence, Phys. Fluids A 5 (8) (1993) 2008–2013.

[18] M. Skote, J. H. Haritonidis, D. S. Henningson, Varicose instabilities in turbulent boundary layers, Phys. Fluids 14 (2002) 2309–2323.